Global and Planetary Change 228 (2023) 104218

Contents lists available at ScienceDirect

Global and Planetary Change

journal homepage: www.elsevier.com/locate/gloplacha

Divergent trends of changes in annual mean and summer temperature in southwestern China during the Holocene

Can Zhang [a], Cheng Zhao [a,b,*], Shi-Yong Yu [c], Bin Xue [a], Xiangdong Yang [a], Yanling Li [a,d], Chengcheng Leng [a], Jun Cheng [e], Ji Shen [a,b]

[a] State Key Laboratory of Lake Science and Environment, Nanjing Institute of Geography and Limnology, Chinese Academy of Science, Nanjing 210008, China
[b] School of Geography and Ocean Science, Nanjing University, Nanjing, 210023, China
[c] School of Geography, Geomatics, and Planning, Jiangsu Normal University, Xuzhou 221116, China
[d] Institute for Ecological Research and Pollution Control of Plateau Lakes, School of Ecology and Environmental Science, Yunnan University, Kunming 650500, P. R. China
[e] Key Laboratory of Meteorological Disaster, Nanjing University of Information Science and Technology, Nanjing 210044, China

ARTICLE INFO

Editor: Dr. Alan Haywood

Keywords:
Seasonal temperature
Holocene
Insolation
Greenhouse gas forcing
Southwestern China

ABSTRACT

Reconstructing Holocene temperature changes in the continental setting is crucial for better assessing the position of recent global warming within the context of long-term natural climate variability and understanding the relationship between temperature changs and monsoon system. However, the pattern and rate of Holocene temperature variations still remain enigmatic due to lack of land-based proxy reconstructions with an unambiguous climatic significance. Here we present a well-dated, high-resolution, quantitative temperature record based on brGDGT proxy during the past 8000 years from the Chenghai Lake in southwestern China. A systematic modern investigation reveals a close correlation between the reconstructed and instrumental mean annual air temperature (MAAT) during the past 60 years, suggesting that sedimentary brGDGT proxy can capture the variations of MAAT during the geological past with a high fidelity. Within an improved chronological framework, our reconstructed Holocene MAAT record displays a long-term warming trend with a magnitude of ~1.5 °C. This overall warming pattern is consistent with the variations of existing regional MAAT records, but in contradiction to the summer temperature records which is similar to the variation of the Asian summer monsoon. In light of state-of-the-art transient climate simulations, we demonstrate that changes in Holocene MAAT were forced by local annual-mean insolation with an additional radiative forcing of greenhouse gases, while changes in summer temperature were mainly controlled by local summer insolation, thereby resulting in a divergent pattern of seasonal temperature changes in southwestern China. Our study provides new evidence for reconciling the "Holocene temperature conundrum" between proxy reconstruction and model simulations from low latitudes.

1. Introduction

The Holocene is the most recent geological epoch in which human civilization emerged and flourished. Quantitative reconstructions of Holocene temperature changes may provide an important knowledge base not only for better understanding the dynamics of the natural climate system, but also for evaluating the position of recent global warming as well as the relationship between climate changes and Neolithic civilization (Tierney et al., 2020; IPCC, 2021). However, our knowledge about the pattern and driving forces of Holocene temperature variations, especially the long-term trend, still remain fragmentary (Renssen et al., 2009; Marcott et al., 2013; Kaufman et al., 2020).

The concept of a cooling trend during the Holocene has been widely accepted, partly as a result of the initial compilation of 73 proxy records worldwide (Marcott et al., 2013). This study further adopts Northern Hemispheric summer insolation as the pace maker of global temperature change known as the "Milankovitch theory". Nevertheless, from the perspective of "conservation of energy", global annual mean radiative forcing should show an increasing trend rather than a decreasing trend during the Holocene. This is because that the net contribution of orbital insolation to the Earth's surface did not change substantially, while the retreating ice sheets and the rising atmospheric greenhouse gases

* Corresponding author at: School of Geography and Ocean Science, Nanjing University, Nanjing 210023, China.
E-mail address: czhao@nju.edu.cn (C. Zhao).

https://doi.org/10.1016/j.gloplacha.2023.104218
Received 30 October 2022; Received in revised form 18 July 2023; Accepted 17 August 2023
Available online 19 August 2023

(GHGs) level led to a long-term increase of radiative forcing during the Holocene (Laskar et al., 2004; IPCC, 2021). Thus, Liu et al. (2014) questioned the reliability of the proxy-based global temperature reconstruction and proposed a globally averaged warming trend based on model simulations. The discrepancy between proxy-reconstructed cooling and model-simulated warming is colloquially referred to as the "Holocene temperature conundrum".

Recently, considerable efforts have been devoted to reconciling this controversy (Park et al., 2019; Bader et al., 2020; Kaufman et al., 2020; Rao et al., 2020). Although the global annual mean insolation remained nearly constant during the Holocene, strong regional variations existed (Laskar et al., 2004). The annual mean incoming solar radiation in the tropics increased in the Holocene, whereas the radiation in the high-latitude regions decreased. Many studies tend to attribute this controversy to the region differences and seasonal bias of the current temperature proxies (Liu et al., 2014; Bova et al., 2021; Osman et al., 2021). For example, Marsicek et al. (2018) revealed that the global dataset displays a Holocene warming trend after removing the proxy records from the North Atlantic realm. Furthermore, a re-assessment of the dataset of Marcott et al. (2013) showed that global mean temperature consistently follows the regional stacks from mid- to high-latitudes of the Northern Hemisphere, different with temperature changes in the tropics (Hou et al., 2019; Zhang et al., 2022a). This finding implies that proxy-based reconstructions in the extratropical regions have a distinct seasonal bias (Park et al., 2019; Bader et al., 2020). Therefore, an effective separation between the summer and annual mean temperature records in the tropics is indispensable (Park et al., 2019), which in turn may reveal distinctly opposite patterns of temperature changes with a seasonal imprint of insolation (Bova et al., 2021). In addition, the latest multi-model simulation reveals the strong sensitivity of temperature changes to local annual insolation in the tropics especially for tropical northern Africa, the southern Arabia Peninsula, India, and southwestern China (Park et al., 2019; Bader et al., 2020). Unfortunately, land-based temperature records in the low latitudes are quite scarce, especially in the areas sensitive to local annual insolation (Zhao et al., 2021a; Zhang et al., 2022b). This emphasized an urgent need for generating more continental temperature records with unambiguous climate signal to be included in the global compilation, especially in the tropics. Model-data comparison is also necessary for an in-depth understanding of Holocene temperature history.

Branched glycerol dialkyl glycerol tetraethers (brGDGTs) have been used as a reliable proxy to reconstruct temperature quantitatively in terrestrial environments such as soils, peats, and lakes (De Jonge et al., 2014; Naafs et al., 2017; Russell et al., 2018; Crampton-Flood et al., 2020; Martinez-Sosa et al., 2021; Zhang et al., 2021). BrGDGTs are membrane-spanning lipids produced by heterotrophic bacteria containing two C_{28} alkyl chains with 4–6 methyl substituents and 0–2 cyclopenthy moieties (Schouten et al., 2013). The utility in temperature reconstructions is based on the capacity of bacteria to alter the fluidity of their lipid membrane to adjust colder/warmer conditions by producing more/less methyl branches (Sinninghe Damsté et al., 2009). Many temperature-calibration equations have been proposed based on the "new method"—which can separate the 5-methyl and 6-methyl brGDGTs—for lake sediments (Table 1). For example, Dang et al. (2018) establishes the calibration equation between growth season temperature and fractional compounds of brGDGTs based on 35 lakes in East China; Russell et al. (2018) establishes the calibration equation between annual mean temperature and brGDGTs-based MBT'$_{5ME}$ indices based on 65 lakes in East Africa, and similar calibration equation was also established for 9 southwest Chinese lake (Zhao et al., 2021a); Martinez-Sosa et al. (2021) further established the calibration equation between annual mean temperature and fractional compounds of brGDGTs based on 261 global lakes. These calibration equations have been successfully applied to reconstruct past temperature changes quantitatively in many regions including the tropics (Feng et al., 2019; Ning et al., 2019; Zhang et al., 2022b).

Table 1
Formulae of brGDGT indices and calibrations for temperature.

Index	Definition/calibration	Reference
MBT'$_{5ME}$	MBT$_{5ME}$ = (Ia + Ib + Ic)/(Ia + Ib + Ic + IIa + IIb + IIc + IIIa+ IIIb + IIIc)	De Jonge et al., 2014
Index1	Index1 = log [(Ia + Ib + Ic + IIa' + IIIa')/(Ic + IIa + IIc + IIIa+ IIIa')]	De Jonge et al., 2014
CBT'	CBT' = log [(Ic + IIa' + IIb' + IIc' + IIIa' + IIIb' + IIIc')/(Ia + IIa + IIIa)]	De Jonge et al., 2014
BIT	BIT = (Ia + IIa + IIa' + IIIa+ IIIa')/(Ia + IIa + IIa' + IIIa+ IIIa' + crenarchaeol)	Hopmans et al., 2004
Growth-season T	Growth T = 12.73–29.73 × [IIIa]$_{5ME}$+ 91.97 × [IIIb]$_{5ME}$ − 551.02 × [IIIc]$_{5ME}$ + 22.65 × [IIb]$_{5ME}$+ 3.19 × [Ib]$_{5ME}$- 4.23 × [IIIa']$_{6ME}$- 147.28 × [IIIb']$_{6ME}$+ 460.1 × [IIIc']$_{6ME}$- 14.59 × [IIa']$_{6ME}$+ 40.02 × [IIb']$_{6ME}$- 230.78 × [IIc']$_{6ME}$+ 7.54 × [Ia]$_{6ME}$+ 29.48 × [Ic]$_{6ME}$ (R^2 = 0.91, RMSE = 1.1 °C)	Dang et al., 2018
MAAT	MAAT = −1.21 + 32.42 × MBT'$_{5ME}$ (R^2 = 0.92, RMSE = 2.44 °C)	Russell et al., 2018
MAAT	MAAT = 12.18 + 19.11 × Index1 (R^2 = 0.92, RMSE = 2.49 °C)	Zhao et al., 2021a
MAAT	MAAT = 14.74–34.46 × [IIIa]$_{5ME}$+ 27.49 × [IIa]$_{5ME}$- 35.36 × [IIb]$_{5ME}$-60.36 × [Ia]$_{5ME}$- 95.91 × [Ib]$_{5ME}$	Martinez-Sosa et al., 2021

In this study, we present two well-dated brGDGT records including one short record with ~ 1-year resolution spanning the last century and one long record with a ~ 50-year resolution spanning the past 8000 year from the Chenghai Lake in southwestern China. We aimed to: (1) quantitatively reconstruct temperature changes since 8000 yr BP based on a brGDGT-temperature calibration equation validated using surface sediments and meteorological data; (2) investigate the pattern of Holocene summer and annual temperature changes in southwestern China; (3) elucidate possible physical causes of Holocene temperature changes in light of the state-of-the-art transient climate simulations from the Community Climate System Model version 3 (CCSM3).

2. Study site

The Chenghai Lake (CH Lake, 26°27′-26°38′N, 100°38′-100°41′E, ~1503 m a.s.l.) is located on the Yunnan-Guizhou Plateau, approximately 18 km southeast of Yongsheng County in Yunnan province, southwestern China (Fig. 1). It is a tectono-fault depression lake formed during the early Pleistocene. This lake has a surface area of ~77.22 km^2, a catchment area of 228.9 km^2, and water volume of 19.87 × 10^8 m^3 (Wang and Dou, 1998). The lake basin is surrounded on three sides by mountains with a broad valley to the south. The mean and maximum water depth of CH Lake are ~ 26 m and ~ 35 m, respectively. At present, it is a hydrologically closed and slightly brackish lake with a salinity of 1.042 g L^{-1} and pH of 8.2. The lake has no perennial inflows and outflows, mainly fed from precipitation on the catchment area and groundwater (Editorial Board of Yongsheng County Annals, 1989).

Currently, the study region is dominated by a warm-temperate mountainous monsoonal climate with distinct rainy and dry seasons. It is mainly influenced by the warm-humid airflow from the Indian Ocean and the Bengal Bay in summer and by the southern branch of the westerly airflow in winter and is also affected by the local climate of the Qinghai-Tibet Plateau. Meteorological data at the nearby Yongsheng station (2130.5 m a.s.l.) show that the mean annual precipitation (MAP) is ~950 mm with ~90% of precipitation falling from June to October over the period of 1981–2010. The mean annual temperature (MAT) is ~13.7 °C with the warmest month of ~19.5 °C and the coldest month of ~6.3 °C without year-round ice cover. The vegetation in the catchment is dominated by *Pinus yunnanensis* forests, coniferous and broadleaved mixed forests, and shrubs (Wang and Dou, 1998).

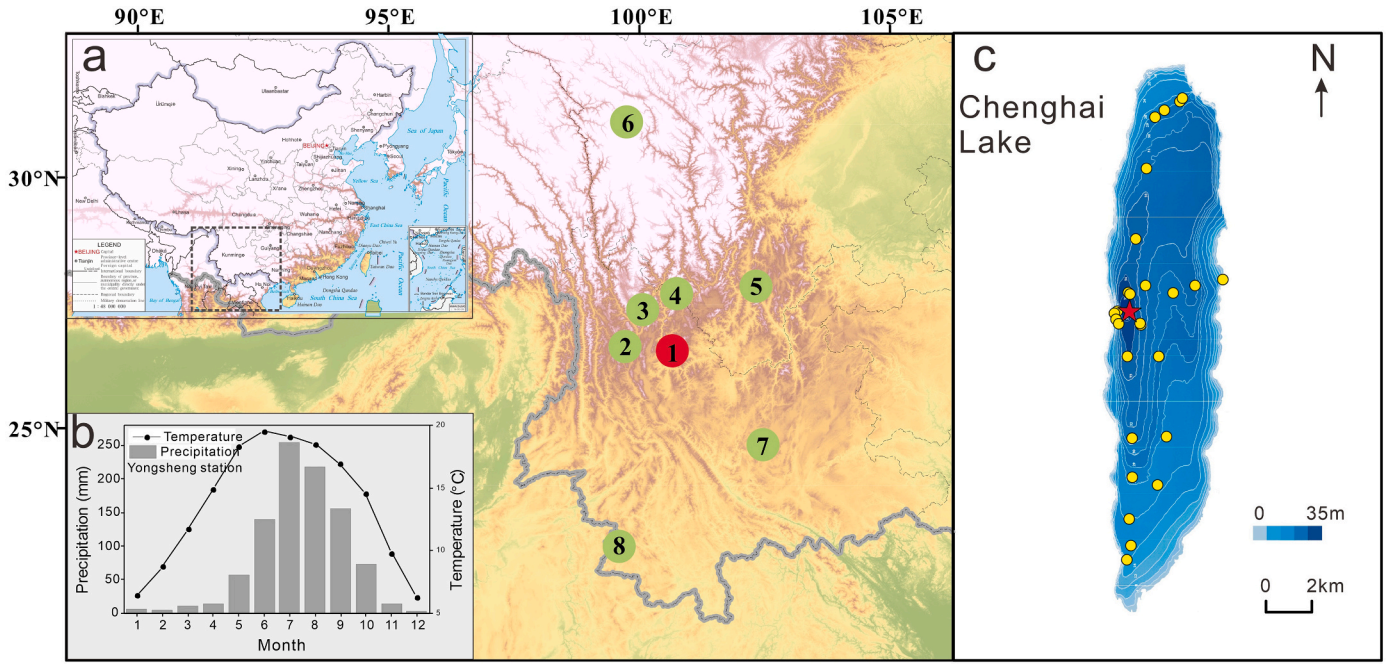

Fig. 1. Location and setting of the Chenghai Lake. (a) Map showing the location of the Chenghai Lake (filled red circle, No.1) and other paleotemperature records (filled green circles) in southwestern China. Nos. 2–8 represent Tiancai Lake (No.2), Heihai Lake (No.3), Lugu Lake (No.4), Qionghai Lake (No.5), Nalengco Lake (No.6), Xingyun Lake (No.7), and Ximenglongtan Lake (No.8). The interior illustration of Fig. 1a show the location of southwest China, which is retrieved from Ministry of Natural Resources of the People's Republic of China (http://bzdt.ch.mnr.gov.cn/download.html). (b) Mean monthly temperature and precipitation (1958–2014) at the Yongsheng Meteorological Station, Yunnan, China (data from the China Meteorological Administration, http://data.cma.cn/). (c) Bathymetry of the Chenghai Lake and locations of the sediment cores (red asterisks), surface sediment samples (yellow dots). (For interpretation of the references to colour in this figure legend, the reader is referred to the web version of this article.)

3. Materials and methods

3.1. Sample collection

In March 2012, a 5.56-m-long sediment core (denoted as CH12) was drilled from the lake center at a water depth of ~31.8 m using a 6-cm inner diameter Piston Corer on a UWITEC platform. The sediment cores were transported to the laboratory in PVC tubes and described and subsampled at every 1-cm interval shortly thereafter and stored at 4 °C repository until analysis. The uppermost 23 cm of the core may have been disturbed, so we only analyzed the sediment between 23 and 556 cm (Li et al., 2015). In fall 2015, a 40-cm-long core (denoted as CH15C), covering the sediment-water interface, was collected from the lake center using a gravity corer and was sampled at 0.5-cm intervals in field. In addition, modern samples including 29 lake surface sediments (uppermost 1 cm) and 7 top soil samples (the uppermost 1 cm) were also collected (Fig. 1).

3.2. Chronology

The dating results of long core CH12 were previously reported by Li et al. (2015). Nine terrestrial plant macrofossils were dated using an accelerator mass spectrometry (AMS—^{14}C) at Beta Laboratory. All the AMS-^{14}C dates were calibrated to calendar ages before present (BP = 1950 CE) using the IntCal13 calibration dataset (Reimer et al., 2013). The depth-age model of long core CH12 were further established using linear interpolation through the midpoints of the two-sigma calibrated age ranges (Li et al., 2015). The short core CH15C was analyzed for ^{210}Pb and ^{137}Cs activities at 0.5-cm intervals using a gamma spectrometer (Hyperpure Ge detector) at the State Key Laboratory of Lake Science and Environment, Nanjing Institute of Geography and Limnology, Chinese Academy of Sciences (NIGLAS). The age-depth relationship of core CHC was established using the constant rate of supply (CRS) model (Appleby and Oldfield, 1978).

3.3. Lipid extraction and brGDGTs analysis

A total of 29 surface samples and 206 sediment samples (141 from long core CH12 and 65 samples from short core CH15C) were analyzed for GDGTs following the procedures described in Zhang et al., 2022b. Freeze-dried and homogenized samples (ca. 5 g) were ultrasonically extracted using dichloromethane: methanol (9:1, v/v, 15 min, 4×). The total lipids were concentrated with N_2 gas and saponified for more than 12 h with 6% KOH in methanol solution. The neutral lipids were extracted using n-hexane for 4 times and then separated into apolar and polar fractions through silica gel column chromatography by n-hexane and MeOH, respectively. The polar fraction, containing the GDGTs, was filtered through a 0.45 μm PTFE filter before analysis.

GDGTs were analyzed using UPLC-APCI-MS (the ACQUITY I-Class plus /Xevo TQ-S system), with full separation of 5- and 6-methyl isomers, equipped with two coupled UPLC silica columns (BEH HILIC columns, 3.0 × 150 mm, 1.7 μm; Waters) in series, fitted with a pre-column at NIGLAS (Zhang et al., 2022b). Samples were brought up in 1000 μL n-hexane injection volume was 5 μL. Samples were eluted with a constant flow rate of 0.4 mL/min for 80 min with 82% *A* and 18% *B* for the first 25 min, where *A* = hexane and *B* = hexane: isopropanol (9:1, *v*/v), followed by a linearly change to 65% *A* and 35% *B* for 25–50 min, and then to 100% *B* for 50–60 min, followed by 20 min wash the column with 84% *A* and 16% *B* to equilibrate the column. The APCI-MS conditions were set up as follows: a probe temperature of 550 °C, voltage corona of 5.0 μV, voltage cone of 110 V, gas flow desolvation of 1000 l/h, gas flow cone of 150 l/h and collision gas flow of 0.15 mL/min. BrGDGTs isomers were detected using selective ion monitoring (SIM) mode via $[M + H]^+$ ions at *m/z* 744 for the C_{46} standard, m/z 1050, 1048, 1046, 1036, 1034, 1032, 1022, 1020 and 1018 for the brGDGTs (De Jonge et al., 2014; Hopmans et al., 2016). The modern samples were

analyzed with the C_{46} standard and the relative concentrations of brGDGTs were calculated according to the integrated peak areas. The formulae for the brGDGT indices and partial calibrations for temperature used in this study are listed in Table 1.

3.4. Data compilation and climate model simulation

To investigate the seasonal pattern of Holocene temperature changes in southwestern China, we review the published quantitative records for summer and annual temperature in the Holocene. The annual temperature records include pollen-inferred temperature at NalengCo Lake, and brGDGT-inferred temperature at Lugu Lake, Qionghai Lake and Ximenlongtan Lake (Opitz et al., 2015; Ning et al., 2019; Zhao et al., 2021a). The summer temperature records include chironomid-inferred temperature at Tianchi Lake and Heihai Lake, pollen-inferred temperature at Xingyun Lake (Chang et al., 2017; Zhang et al., 2017a; Wu et al., 2018). We fully follow the original interpretation of reconstructed temperature in the previous literature, and whether seasonal bias of some reconstructed temperature exists would be further discussed below.

To better understand the possible forcing mechanism of Holocene annual and summer temperature changes in southwestern China, we compare the proxy-reconstructed records and output results from the TraCE-21 ka model project of CCSM3 (Collins et al., 2006). The TraCE-21 ka is the first state-of-art transient simulation of the global climate over the last 21 ka (He, 2011; Liu et al., 2014). The TraCE-21 ka simulation was forced by full forcing and four individual forcings including orbital insolation (ORB), atmospheric greenhouse gas concentrations (GHG), continental ice sheets (ICE), and meltwater flux (MWF). The simulated summer and annual temperature of multipoint-average for these sites mentioned above was calculated for better comparison with the reconstructed temperature records.

4. Results

4.1. Chronology

The chronology of the long core spans the last 8000 years and the sedimentation rate varies between 0.05 and 0.20 cm/yr with a mean of ~0.07 cm/yr (Li et al., 2015). The chronology of the short core spans from 1900 to 2015 CE with a relatively constant sedimentation rate of 0.35 cm/yr (Fig. 2). The average temporal sampling resolution of the GDGT records is ~40 years for the long core CH12 since 8000 yr BP and ~ 1.2 years for the short core during the past century.

4.2. Molecular distributions and concentration of brGDGTs

For lake sediments and catchment soil samples, non-cyclopentane moieties dominate the distribution of brGDGTs. In lake surface sediments, pentamethylated brGDGTs are the most abundant (IIa and IIa', 39.6%), followed by tetramethylated brGDGTs (Ia, 19.1%) and hexamethylated brGDGTs (IIIa and IIIa', 18.7%) (Fig. 3a). Similarly, down-core samples show a distribution pattern similar to that of surface sediments with the highest pentamethylated brGDGTs (IIa and IIa', 32.6%) (Fig. 3b). However, the relative abundance of brGDGTs containing 1–2 cyclopentane moieties is generally low. In contrast, catchment soils show a distribution pattern quite different to those of both surface sediments and down-core samples (Fig. 3c). Ternary diagram of the relative abundance of tetra, penta- and hexamethylated brGDGTs displays a remarkable difference between catchment soils and lake sediments including surface and down-core samples (Fig. 3d). Lake sediments have a greater proportion of the penta-methylated brGDGTs, while catchment soils have a tetra-ethylated dominance. In addition, the concentration of brGDGTs in surface sediments displays a clearly increasing trend with water depth and keeps relatively stable above 20 m (Fig. 3e). BIT value shows no distinct relation with the variation of water depth (Fig. 3f).

The average concentration of brGDGTs is 6322 ng/g in surface sediments, which is about two orders of magnitude higher than that in

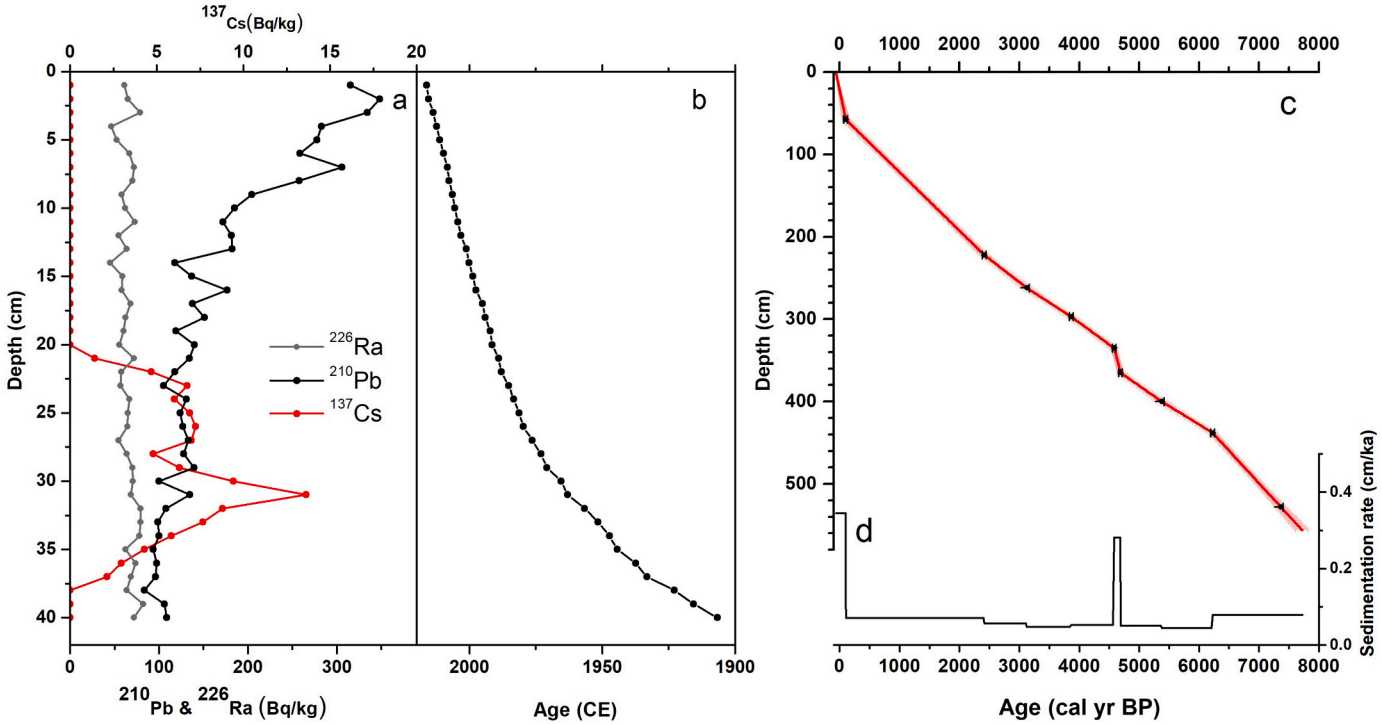

Fig. 2. Chronology of sediment cores. (a) ^{210}Pb, ^{226}Ra, and ^{137}Cs activities (Bq/kg) of dried sediments. (b) Age-depth model of core CH15C established using the CRS (constant rate of supply) model. (c) Age-depth model and (d) sedimentation rate of long core CH12 previously reported by Li et al. (2015).

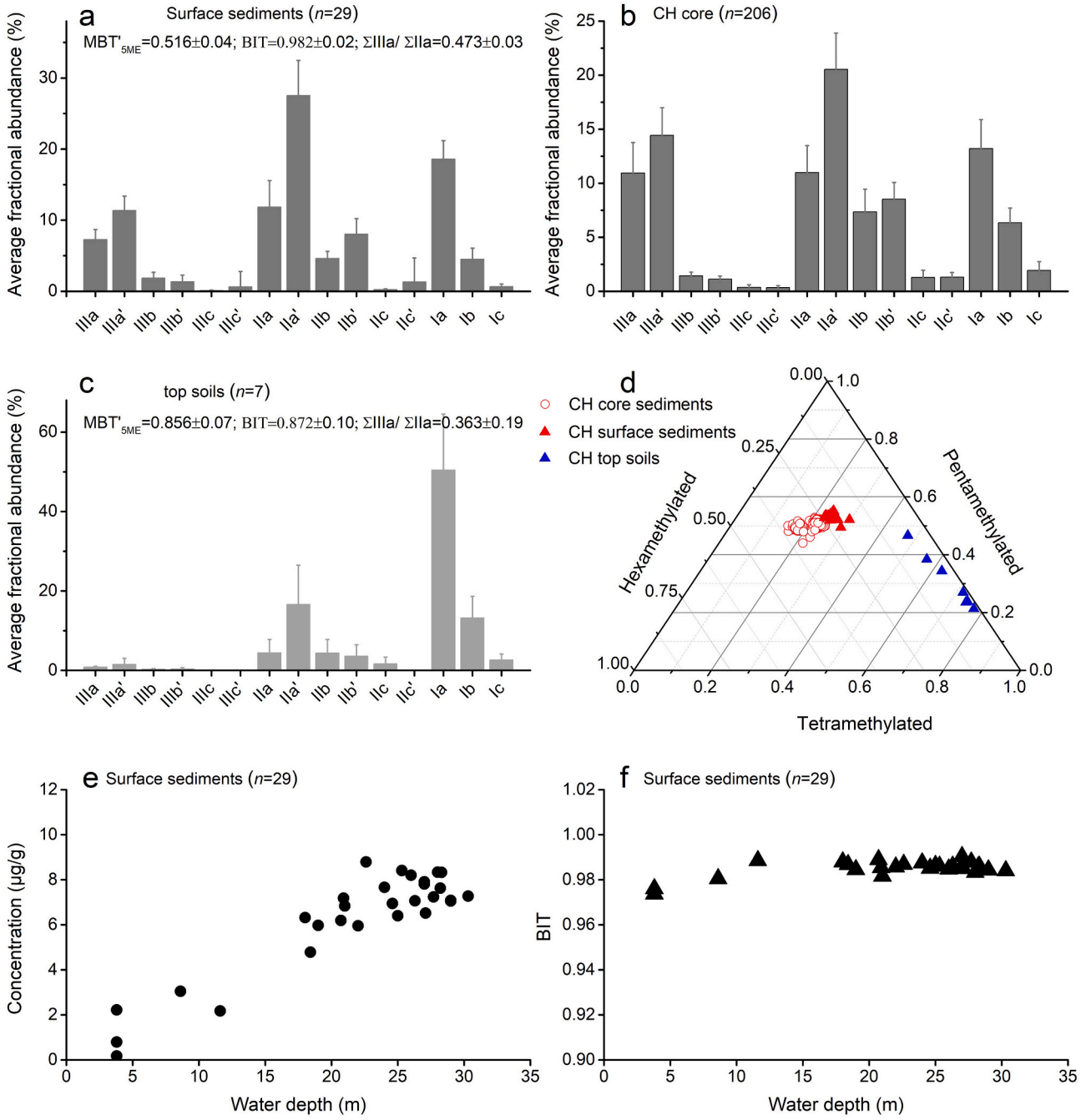

Fig. 3. Distribution and source of brGDGTs in the CH Lake. Average fractional abundance of brGDGTs in (a) surface sediments, (b) down-core sediments, and (c) catchment soils. (d) Ternary plots of the relative abundance of tetramethylated, pentamethylated, and hexamethylated brGDGTs from lake sediments and catchment soils. (e) Relation between water depth and brGDGT concentration of surface sediments. (f) Relation between water depth and Branched and Isoprenoid Tetraether (BIT) index of brGDGT in the CH Lake.

catchment soils (93 ng/g) (Fig. S1). The calculated MBT'$_{5ME}$ varies from 0.5 to 0.53 for surface sediments and from 0.8 to 0.9 for catchment soils. Similarly, the calculated index 1 varies from 0.3 to 0.35 for surface sediments and from 0.72 to 1.3 for catchment soils. The calculated CBT' also shows lower values (varying from −0.16 to −0.12) in surface sediments than those in catchment soils, which have a wider range of0–0.75. Overall, these brGDGT-based proxies such as MBT'5ME, Index 1, and CBT' show a quite large difference between lake sediments and soils without overlap between both including brGDGT concentration and brGDGT-based indices (Fig. S1).

4.3. Variations of brGDGT-based indices and temperature reconstruction

The methylation index of MBT'$_{5ME}$ is relatively low and remains nearly constant before 1980 CE and increases rapidly from 0.35 to 0.66 towards 2015 CE (Fig. 4a). Similarly, the proxy of index 1 also shows a gradually increasing trend from 0.06 to 0.5 since 1980 CE (Fig. 4b). The cyclization ratio of CBT' exhibits a slightly increasing trend from −0.05 to 0.1 between 1900 and 1960 CE, followed by a rapid decrease to −0.25 afterwards (Fig. 4c). The brGDGT-inferred mean annual air temperature (MAAT) record from short core CHC indicates a gradual warming trend since 1980 CE (Fig. 4d), which is remarkably consistent with the long-term trend of reconstructed temperature based on other calibrations

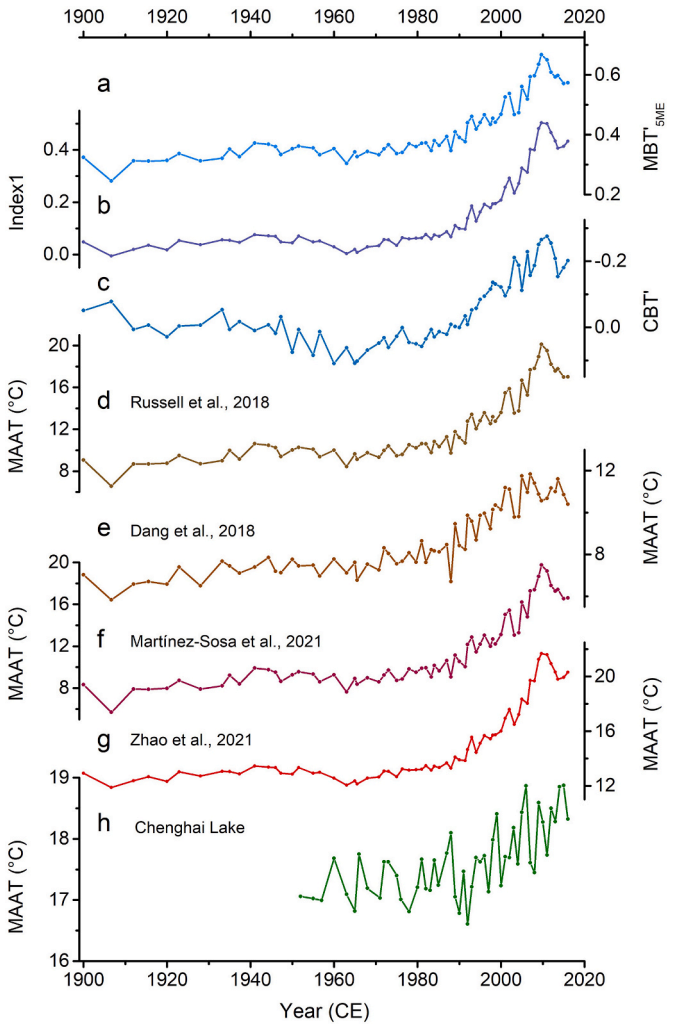

Fig. 4. BrGDGTs proxy and inferred temperature from short core CH15C of the CH Lake. The variations of BrGDGTs proxy including (a) MBT'$_{5ME}$, (b) Index 1, and (c) CBT'. Inferred temperature changes based on recently published global/regional calibration from (d) Russell et al. (2018), (e) Dang et al. (2018), (f) Martinez-Sosa et al. (2021) and (g) Zhao et al. (2021a). (h) Instrumental record of annual mean temperature (MAAT) at the CH Lake inferred from the nearby Yongsheng meteorological station.

and instrumental data (Fig. 4e-h). The brGDGT-inferred MAAT record from long core CH12 displays an overall warming trend with an increase of ~1 °C during the past 7800 years, superposed with several large fluctuations after 3000 yr BP (Fig. 5a).

5. Discussion

5.1. Biological sources of brGDGTs and reconstructed temperature at CH Lake

Previous studies suggest that brGDGT compounds can be produced in both lake sediments and soils (De Jonge et al., 2014; Russell et al., 2018). Therefore, a detailed investigation of brGDGT biological sources is quite necessary before paleotemperature reconstructions based on brGDGT proxy. Our results reveal that the brGDGT distributions of surface sediments are consistent with those of down-core samples at the CH Lake, but distinctly different from catchment soil samples (Fig. 3a-c). The fractional abundance of tetra, penta- and hexamethylated brGDGTs also indicates a remarkable difference between catchment soils and lake sediments including surface and down-core samples (Fig. 3d). The different brGDGT distribution pattern between lake sediments and soils reveals a possible dominating contribution of authigenic production rather than exotic input from catchment soils. It is brGDGTs of lake sediments is predominantly derived from authigenic production that has been widely reported in many previous studies including lakes in southwestern China (Feng et al., 2019; Sun et al., 2021; Zhao et al., 2021a; Zhang et al., 2022b). The conclusion can also be supported by generally increasing concentration of total brGDGTs in surface sediments with increasing water depth and about two orders of magnitude higher than that in soils (Figs. 3-4). A higher brGDGT concentration in lake sediments is also reported at the Towuti Lake (Tiernery and Russell, 2009) and Huguanyan Marr (Hu et al., 2015) which have a authigenic production of brGDGTs. Such an authigenic origin at the CH Lake is supported by a quite large difference of brGDGT-based proxies such as MBT'5ME, Index 1, and CBT' between lake sediments and soils as well (Fig. S1). Thus, all of these lines of evidence demonstrate that brGDGTs in sediments of CH Lake are mainly produced within the water column and/or surface sediments rather than being transported from catchment soils, although the possible soil contributions cannot be completely ruled out.

Considering the authigenic dominance of brGDGTs in CH Lake, the global/regional lake-based calibrations, published in previous studies based on the "new-method", have been applied to our short core to reconstruct temperature changes during the past century (Russell et al., 2018; Dang et al., 2018; Martinez-Sosa et al., 2021; Zhao et al., 2021a). Regarding the overall trend, all of the reconstructed temperature records based on these calibrations display a consistent pattern with a relatively stable and low value between 1900 and 1980 CE, followed by a rapid warming trend since 1980 CE (Fig. 4a-g). The consistent warming trend shows good correlation with instrumental data at a nearby meteorological station (Fig. 4h), which demonstrates that brGDGTs can be used to reconstruct paleotemperature changes at the Chenghai Lake. Nevertheless, the amplitude of reconstructed temperature changes varies significantly from 4 °C to 10 °C for different calibrations, dramatically larger than that of the instrumental temperature record (Fig. 4), which may be ascribed to the size of the GDGT-temperature dataset. The calibration based on large regional and global samples likely leads to a larger amplitude of changes because of the steeper slope between proxy and temperature (Li et al., 2017; Yan et al., 2021). In contrast, the reconstructed temperature based on local correlation shows a smaller amplitude of changes (Feng et al., 2019; Zhang et al., 2022b). Furthermore, we calculated the correlation between the reconstructed and the instrumental temperature records for different calibrations. As shown in Fig. S2, the reconstructed MAAT based on the local calibration from southwest China lakes shows a better correlation ($r = 0.7$, $n = 65$) with the instrumental temperature record than that of other large regional calibrations from East African lakes, East China lakes and global calibrations. This may indicate that the local calibration from southwest China lakes is more appropriate for paleotemperature reconstruction at the Chenghai Lake. Moreover, the inferred core-top temperature (~19.5 °C) based on local calibrations is close to the observed temperature (~19.2 °C) at the nearly Yongsheng weather station after correcting for a regional temperature gradient (He and Wang, 2020). In summary, it is reasonable to apply the local calibration to reconstruct paleotemperature changes at the Chenghai Lake. The brGDGT-inferred MAAT record displays a long-term warming trend with an increase of ~1.5 °C during the Holocene, superposed with several centennial-scale cold events such as at 6600–6400 yr BP, 5100–4800 yr BP, 4100–4000 yr BP, 2400–1900 yr BP, 1500–1200 yr BP, and 600–0 yr BP (Fig. 5a).

5.2. Divergent trends of Holocene reconstructed annual and summer temperature changes in southwestern China

In order to understand the pattern of Holocene temperature changes, we compiled previously published quantitative temperature records in southwestern China. At the annual scale, our reconstructed Holocene

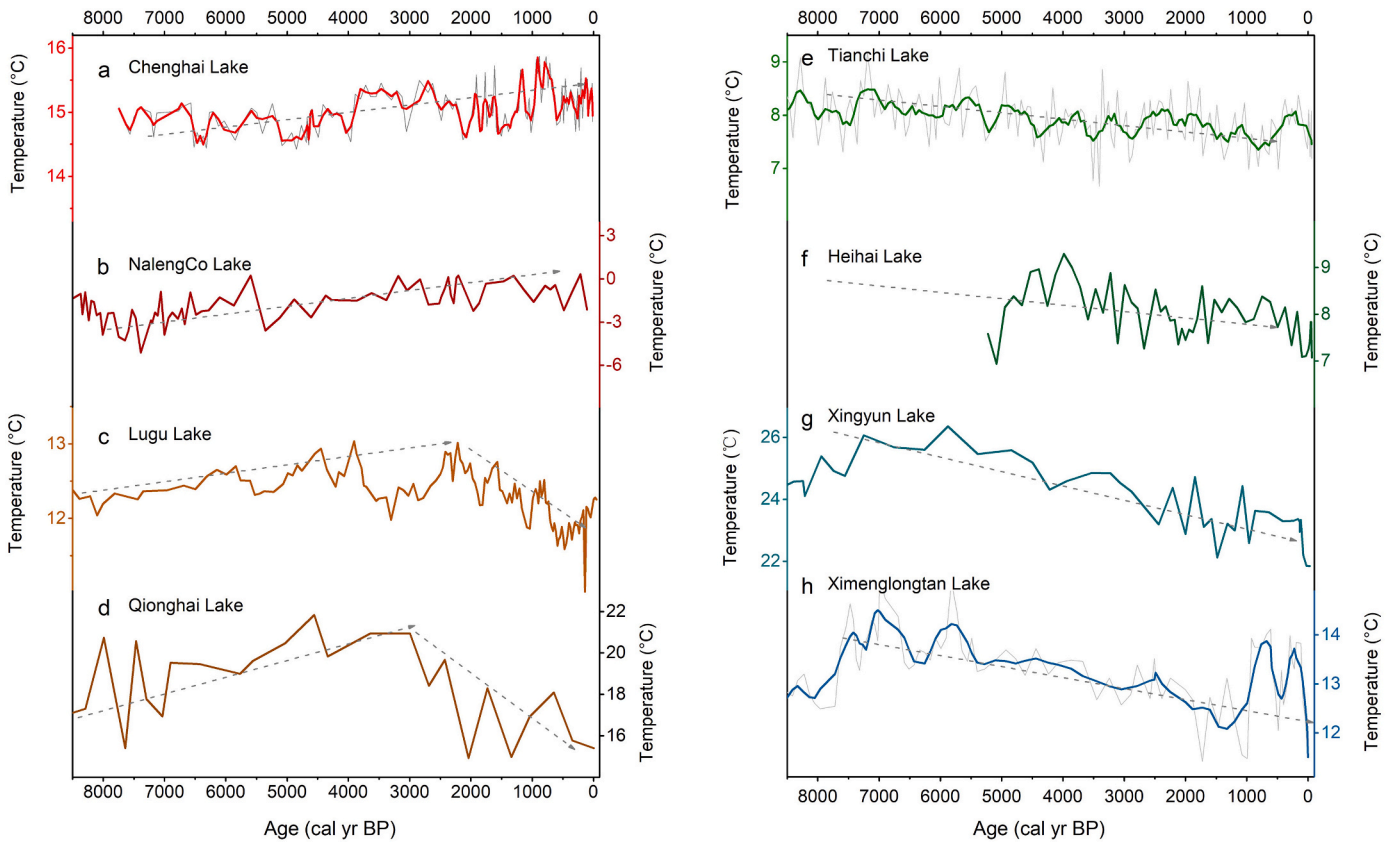

Fig. 5. Compilation of proxy-reconstructed Holocene annual and summer temperature in southwestern China. Reconstructed annual temperature from (a) Chenghai Lake (this study), (b) Nalengcuo Lake (Opitz et al., 2015), (c) Lugu Lake (Zhao et al., 2021a), (d) Qionghai Lake (Wang et al., 2021); Reconstructed summer temperature from (e) Tianchi Lake (Zhang et al., 2017b), (f) Heihai Lake (Chang et al., 2017), (g) Xingyun Lake (Wu et al., 2018), (h) Ximenglongtan Lake (Ning et al., 2019).

temperature at the Chenghai Lake is consistent with many regional published MAAT records (Chen et al., 2020; Zhao et al., 2021a; Zhang et al., 2022b). For example, the pollen-based annual temperature reveals a well-defined warming trend of 2–3 °C over the Holocene at the NalengCo Lake (Fig. 5b). The brGDGT-based annual temperature records also show a gradual warming of ~2 °C at the Lugu Lake and ~ 3 °C at the Qionghai Lake, albeit with a rapid cooling trend after ~2000 yr BP (Fig. 5c-d). Similar trend can be observed for proxy-reconstructed annual temperature at the Tengchongqinghai Lake (Zhao et al., 2021a) and Hongyuan peat (Yan et al., 2021). Note that the late-Holocene cooling may be due to a summer bias of brGDGT-inferred temperature in these lakes, which will be discussed below. Thus, these records consistently indicate an overall long-term warming trend for proxy-reconstructed MAAT records during the Holocene in southwestern China. Regarding the amplitude of temperature changes, most records reveal a 2–3 °C warming such as ~1.5 °C increase for the Chenghai Lake, 2–3 °C increase for the NalengCo Lake, ~2 °C increase for the Lugu Lake, and ~ 3 °C increase for the Qionghai Lake.

In contrast, proxy-reconstructed summer temperature shows a generally cooling pattern during the Holocene in southwestern China. For instance, the chironomid-inferred summer temperature displays a long-term decrease at the Tiancai Lake (Fig. 5e), so does the chironomid-based temperature record at the Heilai Lake (Fig. 5f). The pollen-based summer temperature also exhibits an overall decreasing trend at the Xingyun Lake (Fig. 5g). Similar trend can be observed in the pollen-based summer temperature at the Koucha Lake (Herzschuh et al., 2009) and alkenone-based summer temperature at the Qinghai Lake as well (Hou et al., 2016). This cooling pattern is consistent with the recent pollen-synthesized Holocene summer temperature records in the nearby Tibetan Plateau regions (Chen et al., 2020). Nevertheless, it is noteworthy that there is also an exception with a gradual cooling for brGDGT-based Holocene annual mean temperature at the Ximenglongtan Lake (Fig. 5h). This is likely because that the majority of brGDGTs in this lake are derived from catchment soils with quite limited contributions from in-situ production. Precipitation in southwestern China mainly occurs in the monsoonal season with 80–90% of which falling from June to September, which lead to extensive catchment erosion following the monsoonal precipitation, thereby resulting in a bias of brGDGT-reconstructed summer temperature (Ning et al., 2019). Thus, proxy-based summer temperature records are dominated by a long-term cooling pattern in southwestern China during the Holocene. In addition, the amplitude of reconstructed summer temperature mainly displays a 1–3 °C cooling including 1–2 °C decrease for the Tiancai Lake, Heihai Lake, and Koucha Lake and ~ 3 °C drop for the Xingyun Lake, which is quite close to the change of the synthesized summer temperature record on the Tibetan Plateau (Chen et al., 2020).

The uncertainty on whether seasonal bias in proxy-reconstructed temperature exist should be also considered in our study (Liu et al., 2014; Zhang et al., 2022b). These temperature records mentioned above were mainly reconstructed based on the proxies of chironomid, pollen, and brGDGTs. Firstly, previous study suggests that summer temperature is one of the independent and significant variables for changes in abundance of chironomid species in southwestern China and a calibration was established based chironomid data from 100 lakes (Zhang et al., 2017b). The summer temperature records at Tianchi Lake and Heihai Lake were reconstructed from chironomid species in sediment cores based on this chironomid-temperature calibration (Chang et al., 2017; Zhang et al., 2017b). Secondly, sedimentary fossil pollen was applied to reconstruct summer temperatue at Xingyun Lake, while annual mean temperature at NalengCo Lake. Some studies reveal that fossil pollen

have the potential to reconstruct summer and annual temperatures in different lakes (Davis et al., 2003). Nevertheless, it remains unclear whether or not pollen-inferred temperature has seasonal bias, which may bring some uncertainty for our study and further investigation is needed for reducing the effect of seasonal bias (Zhang et al., 2023). Thirdly, for brGDGT-based reconstructions, many studies indicate brGDGT proxy can well record changes in annual mean temperature in low-latitude including southwestern China because water temperature can covary with local air temperture due to the non-frozen condition throughout the year (Tierney et al., 2010; Russell et al., 2018; Zhao et al., 2021b; Zhang et al., 2022b). The annual mean temperature records were widely reconstructed based on brGDGT proxy at Lugu Lake, Qiong Lake and Ximenglongtan Lake (Ning et al., 2019; Wang et al., 2021; Zhao et al., 2021a). In addition, it is worth noting that these temperature records at Lugu Lake and Qionghai Lake show a remarkable cooling over the past ~2000 yr BP, which is similar to the recent temperature reconstruction for North America and Europe (Marsicek et al., 2018). This may be related to catchment disturbance and vegetation shifts caused by human activities, which possibly result in a severe deviation between actual temperature changes and proxy responses (Wang et al., 2014; Xiao et al., 2014; Liang et al., 2019; Wang et al., 2021). For example, extensive soil erosion related to enhanced human activity and vegetation shifts likely increases the contribution of terrigenous brGDGTs and results in a summer bias of brGDGT-inferred temperature with a cooling trend in the past 2000 yr BP.

In summary, the proxy-reconstructed temperature records exhibit a distinct seasonal difference in southwestern China during the Holocene. The summer temperature displays a long-term cooling pattern, the annual temperature shows a warming trend. For the amplitude of temperature changes, most summer temperature records show a decrease of 1–3 °C, while the annual temperature shows an increase of 2–3 °C.

5.3. *Reconciliation of the divergent trends of Holocene seasonal temperature changes*

In southwestern China, the proxy-reconstructed annual mean

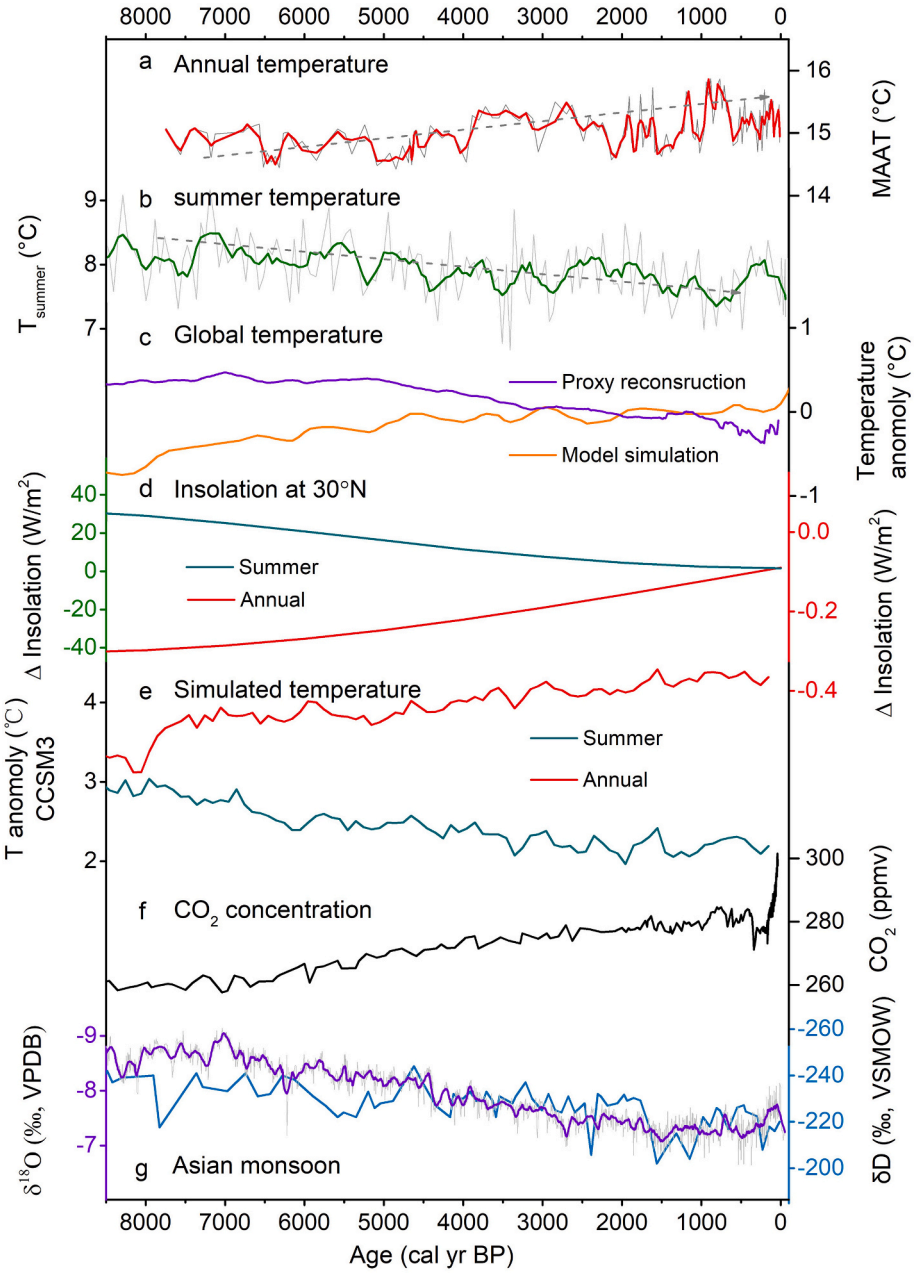

Fig. 6. Comparison of the reconstructed temperature records with climate forcing in southwestern China. (a) Annual temperature from the Chenghai Lake (this study), (b) summer temperature from the Tianchi Lake (Zhang et al., 2017b), (c) global synthesis of proxy-reconstructed temperature (Marcott et al., 2013) and model-simulated global temperature anomaly (Liu et al., 2014). (d) Summer and annual mean insolation at 30°N (Laskar et al., 2004). (e) Simulated summer and annual mean temperature averaged over southwestern China (21°-31° N, 98°-105° E). (f) Dome C ice-core record of the atmospheric CO_2 concentration (Lüthi et al., 2008). (g) Asian summer monsoon inferred from stalagmite$\delta^{18}O$ record of Dongge Cave (Wang et al., 2005) and leaf-waxδD record of Lugu Lake (Zhao et al., 2021b).

temperature records show a warming trend consistent with model-simulated global annual mean temperature sequence (Fig. 6a, c; Liu et al., 2014), which are in pace with the variations of local annual insolation (Fig. 6d). In contrast, the proxy-reconstructed summer temperature records are consistent with the global stacked temperature sequence with distinct summer bias (Fig. 6b, c; Marcott et al., 2013; Marsicek et al., 2018), coherent with changes of summer insolation (Fig. 6d). In order to better understand the possible mechanism of Holocene seasonal temperature changes in southwestern China, the transient climate simulations of TraCE-21 ka project were chosen to compare with the proxy-reconstructed temperature records (Collins et al., 2006; Liu et al., 2009; He, 2011). Model-simulated temperature averaged over southwestern China (21°-31° N, 98°-105° E) under full forcing shows a remarkable similarity with the proxy-reconstructed temperature records not only in the general trend but also in the amplitudes of changes (Fig. 6e). The model results reveal a general cooling summer temperature with a drop of ~1.5 °C and a long-term warming annual temperature with an increase of ~1.5 °C over the Holocene. The good agreement of data-model comparison indicates that the model simulation can well capture temperature variations in southwestern China.

The simulated results were further compared to identify the potential driving mechanisms under full (FULL)-forced and four individual forcings including orbital insolation (ORB), atmospheric greenhouse gas concentrations (GHG), continental ice sheets (ICE), and meltwater flux (MWF). Results suggest that Holocene summer cooling is mainly dominated by the decreasing local summer insolation inferred from the covariation between FULL-forced and ORB-forced temperature with high correlation of $R^2 = 0.83$ (Fig. 7a). However, GHG-forced summer temperature displays a relative stable before ~7000 yr BP and a gradual increase trend afterward, which somewhat even compensates the overall cooling trend of summer temperature (Fig. 6f, Fig. 7a). However, both ICE- and MWF-forced sequences display no apparent variation, indicating the quite limited influences of these two factors. Thus, Holocene cooling of summer temperature is attributed to the dominated drives of summer insolation. This mechanism has also been widely applied for other summer temperature records in southwestern China (Zhang et al., 2017b; Chen et al., 2020), northwestern China (Hou et al., 2016), and northern China (Stebich et al., 2015), and other regions of the Northern Hemisphere (Marcott et al., 2013; Kaufman et al., 2020). Besides, it's worth noting that summer temperature shows a remarkable similarity with the variations of Asian monsoon inferred from stalagmite oxygen isotopes and leaf-wax hydrogen isotopes (Fig. 6g). This indicates that monsoon activity is a summer phenomenon, which mainly reflects summer conditions (Wang et al., 2005; Zhao et al., 2021b).

For the annual temperature, comparing between full driving and four individual forcings indicates that the increasing Holocene annual mean temperature was primarily driven by annual insolation, and the increasing GHGs further promote the overall warming trend after ~7000 yr BP (Fig. 7b). The relatively stable temperature sequences driven by ICE and MWF reveal a limited contribution to Holocene

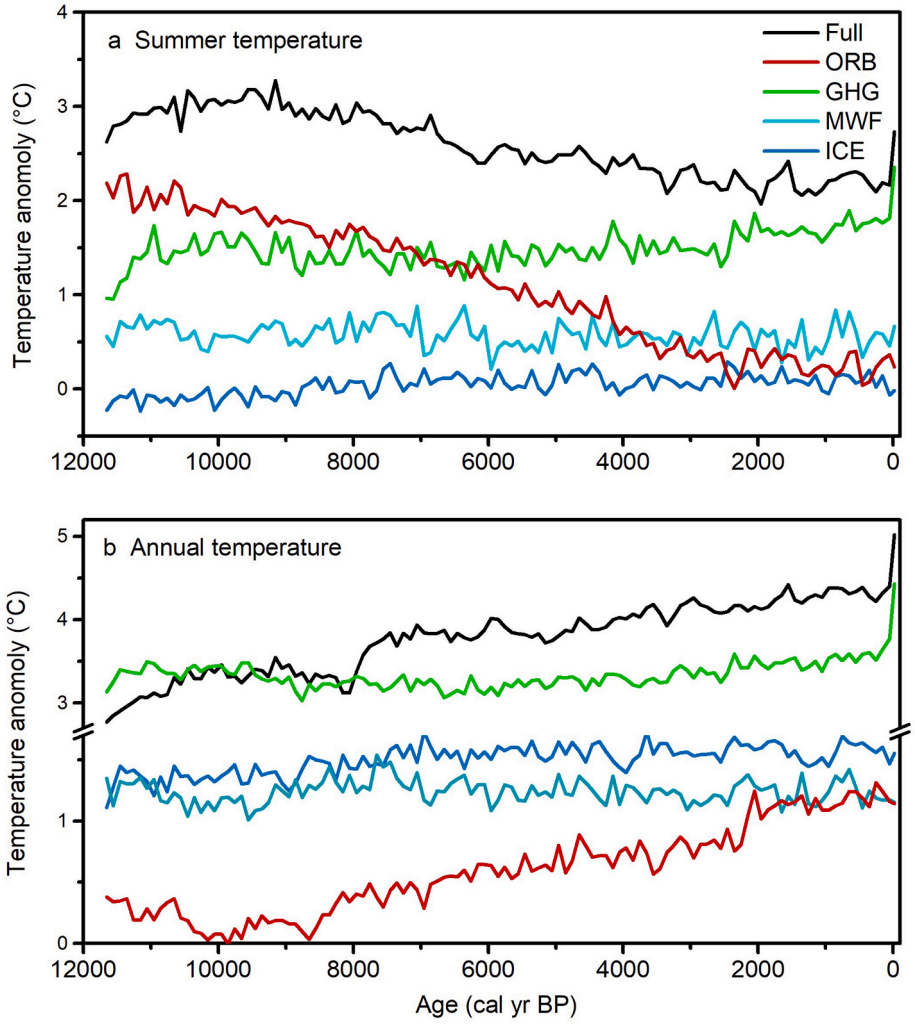

Fig. 7. CCSM3 simulated Holocene temperature changes averaged over southwestern China (21°-31° N, 98°-105° E) under five scenarios of forcing. (a) summer temperature and (b) annual mean temperature. Full = full; GHG = greenhouse gas; ORB = orbital; ICE = ice sheet; MWF = melt water flux.

temperature changes. Furthermore, recent studies also emphasize the synergetic mechanisms of annual insolation and greenhouse gas from proxy-reconstructions in southwestern China (Zhao et al., 2021a) and integrated records on the TP (Zhang et al., 2022b). Nevertheless, there is a difference for the possible driving mechanisms of Holocene overall warming trend between regional records of southwestern China and global data. The long-term warming of simulated global annual temperature was supposed to be in response to the retreating ice sheets and rising GHGs (Liu et al., 2014). At the global scale, the direct net contribution from the orbital insolation to the Earth's surface does not change substantially during the Holocene, and the increase of global annual mean radiative forcing is mainly caused by the retreating ice sheets and rising GHGs, thereby resulting in a globally averaged warming (Liu et al., 2014). In contrast, strong latitude changes of annual mean insolation exist, which can lead to the difference in the spatial pattern of Holocene temperature variation (Laskar et al., 2004). For instance, the annual mean incoming solar radiation in the tropics including our study regions shows a distinct increasing trend over the Holocene, which plays a positive role in the increase of temperature. Indeed, model simulations indicate that the Holocene warming pattern in the tropics was mainly caused by the increased local annual insolation (Liu et al., 2014; Bader et al., 2020; Zhao et al., 2021a). The coupling between Holocene warming in the tropics and local annual insolation was also supported by the average of 13 climate model simulations (Park et al., 2019). The multi-model simulations further emphasized the strong sensitivity of Holocene temperature changes in the tropics to local annual insolation especially for tropical northern Africa, the southern Arabia Peninsula, India, and southwestern China. In addition to the radiative forcing of annual insolation and GHGs, a positive feedback of decreasing monsoon precipitation and regional vegetation changes may also promote the Holocene warming in the tropics, which certainly needs to be tested with additional paleoclimate data and models in the future (Collins et al., 2006; Liu et al., 2014; Bader et al., 2020; Thompson et al., 2022).

Superimposed on this general warming trend, several centennial-scale fluctuations are also recorded in our reconstructed temperature record at the CH Lake (Fig. 6a). Previous researches indicated total solar irradiance (TSI) has been proposed as an important forcing for centennial-scale climate fluctuations (Crowley, 2000; Steinhilber et al., 2012). The power spectral analyses display a significant periodicity at ~240 yr (Fig. S3), which may be related to the ~200 years periodicity of the Suessde Vries cycle in TSI (Suess, 1980), indicating a possible link between TSI and temperature changes. Furthermore, this potential mechanism can be supported by the recent climate simulations based on the Bern 3D-LPJ Earth system model (Roth and Joos, 2013). Besides, other factors such as volcanic activity, north Atlantic cold events, and vegetation feedback may also influence the fluctuations of Holocene temperature and need to be incorporated in future climate simulations (Bond et al., 2001; Sigl et al., 2015; Zhang et al., 2021; Thompson et al., 2022).

In summary, Holocene summer cooling are primarily controlled by local decreasing summertime insolation, while Holocene annual warming was mainly driven by local increasing insolation in southwestern China. The long-term increase of GHGs promote the annual warming, but somewhat compensates the summer cooling. The contributions of ice-sheet and melt-water changes is quite limited for both Holocene summer and annual temperature changes.

6. Conclusions

A detailed modern investigation shows that brGDGTs in the surface sediments of Chenghai Lake are predominantly derived from in-situ production, which reflect the variations of annual mean temperature. The close correlation between the reconstructed temperature based on the local calibration of southwestern China and the instrumental data from a nearby meteorological station supports the applicability of brGDGT proxy for quantitative reconstructions of past temperature changes at the Chenghai Lake.

Our ~50-year-resolution, quantitative, annual mean temperature record displays recurrent centennial-scale fluctuations superimposed on a long-term warming trend with a magnitude of ~1.5 °C during the Holocene. For the long-term trend, the reconstructed Holocene annual mean temperature is consistent with previously published regional temperature records, showing an overall warming pattern with an increase of 2–3 °C. In contrast, the summer temperature displays a long-term cooling pattern with a decrease of 1–3 °C.

The transient climate simulation of TraCE-21 ka project was chosen to further understand the possible mechanism of Holocene temperature changes in southwestern China. Our model-data comparison suggests that the decreasing summer temperature during the Holocene is mainly controlled by local summertime insolation, while the overall increasing annual mean temperature is mainly driven by annual insolation with additional contributions from the rising GHGs level after ~7000 yr BP.

Declaration of Competing Interest

The authors declare that they have no known competing financial interests or personal relationships that could have appeared to influence the work reported in this paper.

Data availability

Data can be obtained in the Supplementary material.

Acknowledgements

We thank A, Zhou, J. Li, X, Feng, and L, Yang for field sampling and laboratory assistance. This work was supported by Natural Science Foundation of China (Grants #42007401, #41877293, #42171151, #42101118, and #42172206), the Program of Global Change and Mitigation (#2016YFA0600502), the Strategic Priority Research Program of Chinese Academy of Sciences (#XDB40000000), and Jiangsu Innovative and Enterpreneurial Talent Programme (JSSCBS20211398).

Appendix A. Supplementary data

Supplementary data to this article can be found online at https://doi.org/10.1016/j.gloplacha.2023.104218.

References

Appleby, P.G., Oldfield, F., 1978. The calculation of lead-210 dates assuming a constant rate of supply of unsupported ^{210}Pb to the sediment. CATENA 5, 1–8. https://doi.org/10.1016/S0341-8162(78)80002-2.

Bader, J., Jungclaus, J., Krivova, N., et al., 2020. Global temperature modes shed light on the Holocene temperature conundrum. Nat. Commun. 11, 4726. https://doi.org/10.1038/s41467-020-18478-6.

Bond, G., Kromer, B., Beer, J., et al., 2001. Persistent solar influence on North Atlantic climate during the Holocene. Science 294, 2130–2136. https://doi.org/10.1126/science.1065680.

Bova, S., Rosenthal, Y., Liu, Z., et al., 2021. Seasonal origin of the thermal maxima at the Holocene and the last interglacial. Nature 589, 548–553. https://doi.org/10.1038/s41586-020-03155-x.

Chang, J., Zhang, E., Liu, E., et al., 2017. Summer temperature variability inferred from subfossil chironomid assemblages from the south-east margin of the Qinghai-Tibetan Plateau for the last 5000 years. The Holocene 27, 1876–1884. https://doi.org/10.1177/0959683617708456.

Chen, F., Zhang, J., Liu, J., et al., 2020. Climate change, vegetation history, and landscape responses on the Tibetan Plateau during the Holocene: a comprehensive review. Quat. Sci. Rev. 243, 106444 https://doi.org/10.1016/j.quascirev.2020.106444.

Collins, W., Bitz, M.C., Blackon, L.M., et al., 2006. The community climate system model version 3 (CCSM3). J. Clim. 19, 2122–2143. https://doi.org/10.1175/JCLI3761.1.

Crampton-Flood, E.D., Tierney, J.E., Peterse, F., et al., 2020. BayMBT: a Bayesian calibration model for branched glycerol dialkyl glycerol tetraethers in soils and peats. Geochim. Cosmochim. Acta 268, 142–159. https://doi.org/10.1016/j.gca.2019.09.043.

Crowley, T.J., 2000. Causes of climate Change over the past 1000 years. Science 289, 270–277. https://doi.org/10.1126/science.289.5477.270.
Dang, X., Ding, W., Yang, H., et al., 2018. Different temperature dependence of the bacterial brGDGT isomers in 35 Chinese lake sediments compared to that in soils. Org. Geochem. 119, 72–79. https://doi.org/10.1016/j.orggeochem.2018.02.008.
Davis, B.S., Brewer, S., Stevenson, A.C., et al., 2003. The temperature of Europe during the Holocene reconstructed from pollen data. Quat. Sci. Rev. 22, 1701–1716. https://doi.org/10.1016/S0277-3791(03)00173-2.
De Jonge, C., Hopmans, E.C., Zell, C.I., et al., 2014. Occurrence and abundance of 6-methyl branched glycerol dialkyl glycerol tetraethers in soils: Implications for palaeoclimate reconstruction. Geochim. Cosmochim. Acta 141, 97–112. https://doi.org/10.1016/j.gca.2014.06.013.
Editorial Board of Yongsheng County Annals, 1989. Yongsheng County Annals. Yunnan People's Publishing House, Kunming (in Chinese).
Feng, X., Zhao, C., D'Andrea, W.J., et al., 2019. Temperature fluctuations during the Common Era in subtropical southwestern China inferred from brGDGTs in a remote alpine lake. Earth Planet. Sci. Lett. 510, 26–36. https://doi.org/10.1016/j.epsl.2018.12.028.
He, F., 2011. Simulating Transient Climate Evolution of the Last Deglaciation with CCSM3. PhD thesis. University of Wisconsin-Madison.
He, Y., Wang, K., 2020. Contrast patterns and trends of lapse rates calculated from near surface air and land surface temperatures in China from 1961 to 2014. Sci. Bull. 65, 1217–1224. https://doi.org/10.1016/j.scib.2020.04.001.
Herzschuh, U., Kramer, A., Mischke, S., et al., 2009. Quantitative climate and vegetation trends since the late glacial on the northeastern Tibetan Plateau deduced from Koucha Lake pollen spectra. Quat. Res. 2009 (71), 162–171. https://doi.org/10.1016/j.yqres.2008.09.003.
Hopmans, E.C., Schouten, S., Sinninghe Damst'e, J.S., 2016. The effect of improved chromatography on GDGT-based palaeoproxies. Org. Geochem. 93, 1–6. https://doi.org/10.1016/j.orggeochem.2015.12.006.
Hopmans, E.C., Weijers, J.H., Schefuß, E., et al., 2004. A novel proxy for terrestrial organic matter in sediments based on branched and isoprenoid tetraether lipids. Earth Planet. Sci. Lett. 224, 107–116. https://doi.org/10.1016/j.epsl.2004.05.012.
Hou, J., Huang, Y., Zhao, J., et al., 2016. Large Holocene summer temperature oscillations and impact on the peopling of the northeastern Tibetan Plateau. Geophys. Res. Lett. 43, 1323–1330. https://doi.org/10.1002/2015gl067317.
Hou, J., Li, C., Lee, S., 2019. The temperature record of the Holocene: progress and controversies. Sci. Bull. 64, 565–566. https://doi.org/10.1016/j.scib.2019.02.012.
Hu, J.F., Zhou, H.D., Peng, P.A., et al., 2015. Reconstruction of a paleotemperature record from 0.3–3.7 ka for subtropical South China using lacustrine branched GDGTs from Huguangyan Maar. Paleogeogr. Paleocl. 435, 167–176. https://doi.org/10.1016/j.palaeo.2015.06.014.
IPCC, 2021. Summary for policymakers. In: Climate Change 2021: The Physical Science Basis. Contribution of Working Group I to the Sixth Assessment Report of the Intergovernmental Panel on Climate Change. Cambridge University Press, Cambridge, United Kingdom and New York.
Kaufman, D., McKay, N., Routson, C., et al., 2020. A global database of Holocene paleotemperature records. Sci. Data 7, 115. https://doi.org/10.1038/s41597-020-0445-3.
Laskar, J., Robutel, P., Joutel, F., et al., 2004. A long-term numerical solution for the insolation quantities of the Earth. Astron. Astrophys. 428, 261–285. https://doi.org/10.1051/0004-6361:20041335.
Li, Y., Liu, E., Xiao, X., et al., 2015. Diatom response to Asian monsoon variability during the Holocene in a deep lake at the southeastern margin of the Tibetan Plateau. Boreas 44, 785–793.
Li, X., Wang, M., Zhang, Y., et al., 2017. Holocene climatic and environmental change on the western Tibetan Plateau revealed by glycerol dialkyl glycerol tetraethers and leaf wax deuterium-to-hydrogen ratios at Aweng Co. Quat. Res. 87, 455–467. https://doi.org/10.1017/qua.2017.9.
Liang, J., Russell, J.M., Xie, H., et al., 2019. Vegetation effects on temperature calibrations of branched glycerol dialkyl glycerol tetraether (brGDGTs) in soils. Org. Geochem. 127, 1–11. https://doi.org/10.1016/j.orggeochem.2018.10.010.
Liu, Z., Otto-Bliesner, B.L., He, F., et al., 2009. Transient simulation of last deglaciation with a new mechanism for Bolling-Allerod warming. Science 325, 310–314. https://doi.org/10.1126/science.1171041.
Liu, Z., Zhu, J., Rosenthal, Y., et al., 2014. The Holocene temperature conundrum. Proc. Natl. Acad. Sci. 111, E3501–E3505. https://doi.org/10.1073/pnas.1407229111.
Lüthi, D., Le Floch, M., Bereiter, B., et al., 2008. High-resolution carbon dioxide concentration record 650,000–800,000 years before present. Nature 453, 379–382. https://doi.org/10.1038/nature06949.
Marcott, S.A., Shakun, J.D., Clark, P.U., et al., 2013. A Reconstruction of Regional and Global Temperature for the past 11,300 years. Science 339, 1198–1201.
Marsicek, J., Shuman, B.N., Bartlein, P.J., et al., 2018. Reconciling divergent trends and millennial variations in Holocene temperatures. Nature 554, 92–96.
Martinez-Sosa, P., Tierney, E.J., Stefanescu, C.I., et al., 2021. A global Bayesian temperature calibration for lacustrine brGDGTs. Geochim. Cosmochim. Acta 305, 87–105. https://doi.org/10.1016/j.gca.2021.04.038.
Naafs, B.A., Inglis, G.N., Zheng, Y., et al., 2017. Introducing global peatspecific temperature and pH calibrations based on brGDGT bacterial lipids. Geochim. Cosmochim. Acta 208, 285–301. https://doi.org/10.1016/j.gca.2017.01.038.
Ning, D., Zhang, E., Shulmeister, J., et al., 2019. Holocene mean annual air temperature (MAAT) reconstruction based on branched glycerol dialkyl glycerol tetraethers from Lake Ximenglongtan, southwestern China. Org. Geochem. 133, 65–76. https://doi.org/10.1016/j.orggeochem.2019.05.003.
Opitz, S., Zhang, C., Herzschuh, U., Mischke, S., 2015. Climate variability on the southeastern Tibetan Plateau since the Lateglacial based on a multiproxy approach from Lake Naleng-comparing pollen and non-pollen signals. Quat. Sci. Rev. 115, 112–122. https://doi.org/10.1016/j.quascirev.2015.03.011.
Osman, M.B., Tierney, J.E., Zhu, J., et al., 2021. Globally resolved surface temperatures since the last Glacial Maximum. Nature 599, 239–244. https://doi.org/10.1038/s41586-021-03984-4.
Park, H.S., Kim, S.J., Stewart, A.L., et al., 2019. Mid-Holocene Northern Hemisphere warming driven by Arctic amplification. Sci. Adv. 5, eaax8203. https://doi.org/10.1126/sciadv.aax8203.
Rao, Z., Shi, F., Li, Y., et al., 2020. Long-term winter/summer warming trends during the Holocene revealed by α-cellulose $\delta^{18}O/\delta^{13}C$ records from an alpine peat core from Central Asia. Quat. Sci. Rev. 232, 106217 https://doi.org/10.1016/j.quascirev.2020.106217.
Reimer, P.J., Bard, E., Bayliss, A., et al., 2013. IntCal13 and Marine13 Radiocarbon Age Calibration Curves 0–50,000 Years cal BP, 4, pp. 1869–1887. https://doi.org/10.2458/azu_js_rc.55.16947.
Renssen, H., Seppä, H., Heiri, O., et al., 2009. The spatial and temporal complexity of the Holocene thermal maximum. Nat. Geosci. 2, 411–414.
Roth, R., Joos, F., 2013. A reconstruction of radiocarbon production and total solar irradiance from the Holocene 14C and CO2 records: implications of data and model uncertainties. Clim. Past 9, 1879–1909. https://doi.org/10.5194/cp-9-1879-2013.
Russell, J.M., Hopmans, E.C., Loomis, S.E., et al., 2018. Distributions of 5- and 6-methyl branched glycerol dialkyl glycerol tetraethers (brGDGTs) in East African lake sediment: Effects of temperature, pH, and new lacustrine paleotemperature calibrations. Org. Geochem. 117, 56–69. https://doi.org/10.1016/j.orggeochem.2017.12.003.
Schouten, S., Hopmans, E.C., Sinninghe Damsté, J.S., 2013. The organic geochemistry of glycerol dialkyl glycerol tetraether lipids: a review. Org. Geochem. 54, 19–61. https://doi.org/10.1016/j.orggeochem.2012.09.006.
Sigl, M., Winstrup, M., McConnell, J.R., et al., 2015. Timing and climate forcing of volcanic eruptions for the past 2,500 years. Nature 523, 543e549. https://doi.org/10.1038/nature14565.
Sinninghe Damsté, J.S., Ossebaar, J., Abbas, B., et al., 2009. Fluxes and distribution of tetraether lipids in an equatorial African lake: Constraints on the application of the TEX86 palaeothermometer and BIT index in lacustrine settings. Geochim. Cosmochim. Acta 73, 4232–4249. https://doi.org/10.1016/j.gca.2009.04.022.
Stebich, M., Rehfeld, K., Schlutz, F., et al., 2015. Holocene vegetation and climate dynamics of NE China based on the pollen record from Sihailongwan Maar Lake. Quat. Sci. Rev. 124, 275–289. https://doi.org/10.1016/j.quascirev.2015.07.021.
Steinhilber, F., Abreu, J.A., Beer, J., et al., 2012. 9,400 years of cosmic radiation and solar activity from ice cores and tree rings. Proc. Natl. Acad. Sci. U. S. A. 109, 5967–5971. https://doi.org/10.1073/pnas.1118965109.
Suess, S.L.G.W., 1980. Correlated variations of planetary albedos and coincident solar-interplanetary variations. Sol. Phys. 68, 393–409. https://doi.org/10.1007/BF00156877.
Sun, X., Zhao, C., Zhang, C., et al., 2021. Seasonality in Holocene temperature reconstructions in Southwestern China. Paleoceanogr. Paleoclimatol. 36 https://doi.org/10.1029/2020PA004025 e2020PA004025.
Thompson, J.A., Zhu, J., Poulsen, J.C., et al., 2022. Northern Hemisphere vegetation change drives a Holocene thermal maximum. Sci. Adv. 8, eabjj6535 https://doi.org/10.1126/sciadv.abj6535.
Tiernery, J.E., Russell, J.M., 2009. Distributions of branched GDGTs in a tropical lake system: Implications for lacustrine application of the MBT/CBT paleoproxy. Org. Geochem. 40, 1032–1036. https://doi.org/10.1016/j.orggeochem.2009.04.014.
Tierney, J.E., Russell, J.M., Eggermont, H., et al., 2010. Environmental controls on branched tetraether lipid distributions in tropical East African lake sediments. Geochim. Cosmochim. Acta 74, 4902–4918. https://doi.org/10.1016/j.gca.2010.06.002.
Tierney, J.E., Zhu, J., King, J., et al., 2020. Glacial cooling and climate sensitivity revisited. Nature 584, 569–573. https://doi.org/10.1038/s41586-020-2617-x.
Wang, S., Dou, H., 1998. Lakes in China, 580 pp. Science Press, Beijing (in Chinese).
Wang, Y., Cheng, H., Edwards, R.L., et al., 2005. The Holocene Asian monsoon: links to solar changes and North Atlantic climate. Science 308, 854–857. https://doi.org/10.1126/science.1106296.
Wang, Q., Yang, X., Anderson, N.J., et al., 2014. Diatom response to climate forcing of a deep, alpine lake (Lugu Hu, Yunnan, SW China) during the last Glacial Maximum and its implications for understanding regional monsoon variability. Quat. Sci. Rev. 86, 1–12. https://doi.org/10.1016/j.quascirev.2013.12.024.
Wang, G., Wang, Y., Wei, Z., et al., 2021. Reconstruction of temperature and precipitation spanning the past 28 kyr based on branched tetraether lipids from Qionghai Lake, southwestern China. Palaeogeogr. Palaeoclimatol. Palaeoecol. 562, 110094 https://doi.org/10.1016/j.palaeo.2020.110094.
Wu, D., Chen, X., Lv, F., et al., 2018. Decoupled early Holocene summer temperature and monsoon precipitation in Southwest China. Quat. Sci. Rev. 193, 54–67. https://doi.org/10.1016/j.quascirev.2018.05.038.
Xiao, X., Haberleb, S.G., Shen, J., et al., 2014. Latest Pleistocene and Holocene vegetation and climate history inferred from an alpine lacustrine record, northwestern Yunnan Province, southwestern China. Quat. Sci. Rev. 86, 35–48. https://doi.org/10.1016/j.quascirev.2013.12.023.
Yan, T., Zhao, C., Yan, H., et al., 2021. Elevational differences in Holocene thermal maximum revealed by quantitative temperature reconstructions at ~30° N on eastern Tibetan Plateau. Palaeogeogr. Palaeoclimatol. Palaeoecol. 570, 110364 https://doi.org/10.1016/j.palaeo.2021.110364.
Zhang, E., Chang, J., Cao, Y., et al., 2017a. Holocene high-resolution quantitative summer temperature reconstruction based on subfossil chironomids from the southeast margin of the Qinghai-Tibetan Plateau. Quat. Sci. Rev. 165, 1–12. https://doi.org/10.1016/j.quascirev.2017.04.008.

Zhang, E., Chang, J., Cao, Y., et al., 2017b. A chironomid-based mean July temperature inference model from the south-east margin of the Tibetan Plateau, China. Clim. Past 13, 185–199. https://doi.org/10.5194/cp-13-185-2017.

Zhang, C., Zhao, C., Zhou, A., et al., 2021. Quantification of temperature and precipitation changes in northern China during the "5000-year" Chinese history. Quat. Sci. Rev. 255, 106819 https://doi.org/10.1016/j.quascirev.2021.106819.

Zhang, W., Wu, H., Geng, J., et al., 2022a. Model-data divergence in global seasonal temperature response to astronomical insolation during the Holocene. Sci. Bull. 67, 25–28. https://doi.org/10.1016/j.scib.2021.09.004.

Zhang, C., Zhao, C., Yu, S., et al., 2022b. Seasonal imprint of Holocene temperature reconstruction on the Tibetan Plateau. Earth Sci. Rev. 226, 103927 https://doi.org/10.1016/j.earscirev.2022.103927.

Zhang, X., Zheng, Z., Huang, K., et al., 2023. Quantification of Asian monsoon variability from 68 ka BP through pollen-based climate reconstruction. Sci. Bull. 68, 713–722. https://doi.org/10.1016/j.scib.2023.03.013.

Zhao, C., Rohling, E.J., Liu, Z., et al., 2021a. Possible obliquity-forced warmth in southern Asia during the last glacial stage. Sci. Bull. 66, 1136–1145. https://doi.org/10.1016/j.scib.2020.11.016.

Zhao, C., Cheng, J., Wang, J., et al., 2021b. Paleoclimate significance of Reconstructed Rainfall Isotope changes in Asian Monsoon Region. Geophys. Res. Lett. 48, e2021GL092460 https://doi.org/10.1029/2021GL092460.